Chemical Engineering Journal Advances 22 (2025) 100762

Contents lists available at ScienceDirect

Chemical Engineering Journal Advances

journal homepage: www.sciencedirect.com/journal/chemical-engineering-journal-advances

Low-temperature Highly Graphitized Porous Biomass-based Carbon as an Efficient and Stable Electrode for Lithium-ion Batteries and Supercapacitors

Sruthy E S [a,b], Alejandro Grimm [b,*], Menestreau Paul [b,c], Christie Thomas Cherian [a], Mikael Thyrel [b], Palanivel Molaiyan [d], Ulla Lassi [d,e], Shaikshavali Petnikota [b], Glaydson Simões Dos Reis [f,*]

[a] School of Electronic Systems and Automation, Digital University Kerala, Thiruvananthapuram, India
[b] Biomass Technology Centre, Department of Forest Biomaterials and Technology, Swedish University of Agricultural Sciences, SE, 90183, Umeå, Sweden
[c] Public Research University Engineering School, IMT Mines Albi, Albi, 81000, France
[d] Research Unit of Sustainable Chemistry, University of Oulu, PO Box 3000, Oulu, FI, 90014, Finland
[e] University of Jyvaskyla, Kokkola University Consortium Chydenius, PO Box 567, Kokkola, FI, 67100, Finland
[f] Laboratory of Industrial Chemistry and Reaction Engineering, Faculty of Science and Engineering, Åbo Akademi University, 20500, Åbo/Turku, Finland

ARTICLE INFO

Keywords:
Logging residue
Koh activation
Porous graphitic carbon
Electrodes/anodes
Lithium-ion batteries
Supercapacitors

ABSTRACT

Graphite is a widely used fossil material valued for its versatility, thanks to its excellent thermal and electrical conductivity as well as high chemical stability. Producing graphitic carbon from biomass offers a promising alternative to fossil graphite, but the process requires extremely high temperatures—up to 3000 °C—leading to significant energy consumption. In this work, we report a greener and more sustainable low-temperature method (900 °C) for the synthesis of highly graphitized biomass carbon using pure boron as a catalyst and logging residues (LR) as a carbon source. The work focuses on the correlation between the structural transformation of the precursors into graphitic carbon and their corresponding electrochemical characteristics as electrodes for lithium-ion batteries (LIBs) and supercapacitors. The carbons were prepared in two steps, i.e., carbonization at 500 °C with boron, followed by activation with KOH at 900 °C. A control carbon, produced using the same method but without boron, was used for comparison. The physicochemical characterization results demonstrated the successful graphitization of the LR-based carbon. In addition, the carbon materials exhibited highly porous structures with specific surface areas (BET) of 2645 $m^2 g^{-1}$ for the boron-treated carbon (BCLR), and 3141 $m^2 g^{-1}$ for the control carbon (CLR). The CLR and BCLR electrodes tested in LIBs delivered specific capacities of 386 and 505 mAh g^{-1} at a 1 C rate at the end of 200 cycles, respectively. CLR and BCLR electrodes were also tested for supercapacitors, delivering specific capacitances of 87 and 144 F g^{-1} at a current rate of 1 A g^{-1}, respectively. This work opens a gateway for a straightforward and cost-effective synthesis method for scaling up biomass-based carbon electrodes for LIBs and supercapacitors, facilitating sustainable precursors and an industrially viable approach.

1. Introduction

Rechargeable lithium-ion batteries (LIBs) are today the leading choice for portable electronic devices and electric vehicles. However, the increasing demand for clean energy makes further research and development of LIBs essential. Similarly, supercapacitors play a key role in energy-related applications, offering exceptional power density, long cycle life, and rapid charging capabilities [1]. Beyond LIBs, supercapacitors are widely used in backup power systems, electric vehicles, and hybrid electric vehicles [2,3]. Carbon-based materials have been extensively explored as anode materials for lithium-ion batteries and electrode materials in supercapacitors [4,5], attributed to their superior conductivity, cost-effectiveness, diverse structure, and natural abundance [6]. Graphite has been predominant among them owing to its remarkable electrochemical stability, lower lithium intercalation potential, and high conductivity [7,8]. Nevertheless, the critical supply of natural graphite, the need for high-temperature graphitization to synthesize artificial graphite, and the low theoretical capacity of 372 mAh

* Corresponding authors.
E-mail addresses: Alejandro.Grimm@slu.se (A. Grimm), Glaydson.SimoesdosReis@abo.fi (G.S.D. Reis).

https://doi.org/10.1016/j.ceja.2025.100762

Available online 22 April 2025

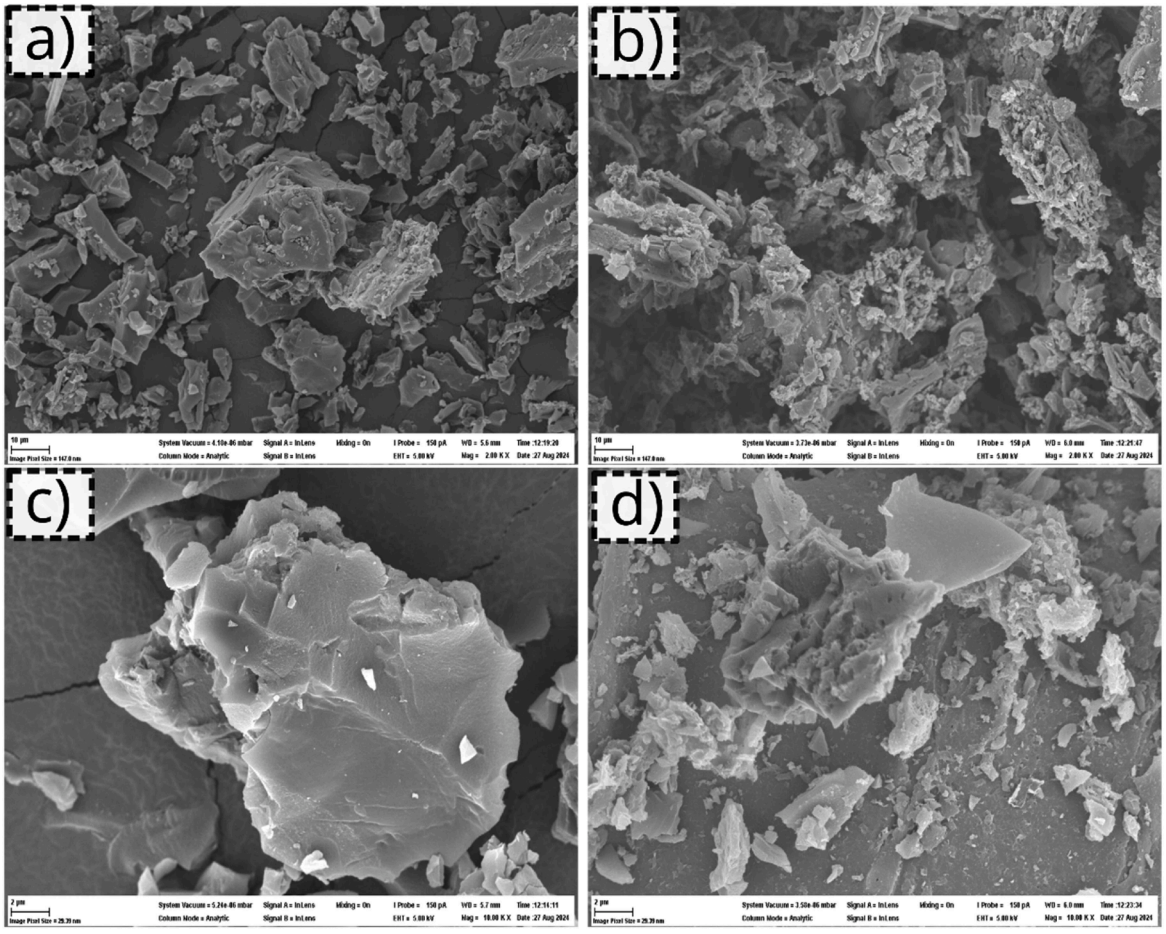

Fig. 1. a) SEM of CLR at 2 K of magnification, b) SEM of BCLR at 2 K of magnification, c) SEM of CLR at 10 K of magnification, d) SEM of BCLR at 10 K of magnification.

g^{-1} are forcing researchers to explore other promising alternatives [7,9]. In the case of supercapacitors, various carbon materials have been explored to date as electrochemical double-layer capacitor (EDLC) electrodes, including graphene, templated carbon, and carbon nanotubes [4]. However, the intricate production process is stagnating the development of several such electrode materials. The demand for graphite is high, and the graphite market is expected to reach around ~ USD 21.6 billion by 2027, due to its multifunctional application in photovoltaics, electronics, and energy storage devices such as supercapacitors and batteries [10,11]. Therefore, more sustainable strategies are required to meet the high demand for graphite. Graphite can be sustainably produced from biomass resources; however, the process is energy-intensive, as it is produced at very high temperatures.

In pursuit of a viable solution to these bottlenecks, biomass-derived activated carbons are drawing attention due to their capability of replacing graphite as an anode material in LIBs and different types of carbons used in supercapacitors [12–15]. The intrinsic molecular structures and architectures of biomass precursors are highly sought-after in battery applications as they are favorable for charge transport and storage [16,17]. Therefore, different biomass precursors, such as rice husk [18,19], peanut shells [20], shells of broad bean [21], lignin [22], olive and cherry stones [23], gelatin [24], spent coffee grounds [25], and cotton [26] have been investigated so far for deriving carbonaceous anode materials for LIBs. These biomass-derived carbons were able to impart higher capacity and cycling stability as anode materials to LIBs. Recent works of literature have reported different ranges of specific capacities, depending on the biomass precursors chosen for LIB anodes. Among them, carbon derived from spent coffee grounds delivered a reversible capacity of 285 mAh g^{-1} at 0.1 A g^{-1} over 100 cycles [25]. A specific capacity of 460.4 mAh g^{-1} has been illustrated in carbon anodes developed from plane tree leaves at a current density of 50 mA g^{-1} in LIBs [27]. Besides, studies have shown that boron-treating electrode samples significantly improve the electrochemical properties, as is evident in the work demonstrated by Kim et al. [28], where they prepared boron-doped carbon from pyrolysis fuel oil which showed a reversible capacity of 301 mAh g^{-1} at a current density of 0.1 C.

Aiming to enhance the graphitization of biomass-based carbon, many catalysts based on Fe, Co, Ni, and Mn have been utilized [29–32]. Non-metal catalysts, such as boron are a sustainable, efficient, and environment-friendly alternative to replace toxic and expensive metals. The use of boron catalysts greatly enhances the graphitization process at relatively low temperatures, thereby improving the electrochemical performance of various electrode materials [33]. It is well known that chemical activation of carbon with KOH as an activation agent helps to develop a highly porous network with high specific surface area that may lead to superior electrochemical properties [34]. The activation process with potassium hydroxide proceeds via complex chemical activation mechanisms that involve the formation of K_2O_3, K_2O, and metallic K. During pyrolysis at high temperatures, water vapor and gases such as CO_2 and CO are generated, which also helps during the process to develop a porous carbon matrix [35]. Herein, the graphitic activated carbon was synthesized from pine tree logging residues using boron as a graphitization catalyst and a facile two-step carbonization process with KOH activation at temperatures of 900 °C, i.e., significantly lower than temperatures employed for producing graphite from biomass-carbon via heat treatments at around 2400 - 3000 °C. The produced graphitized

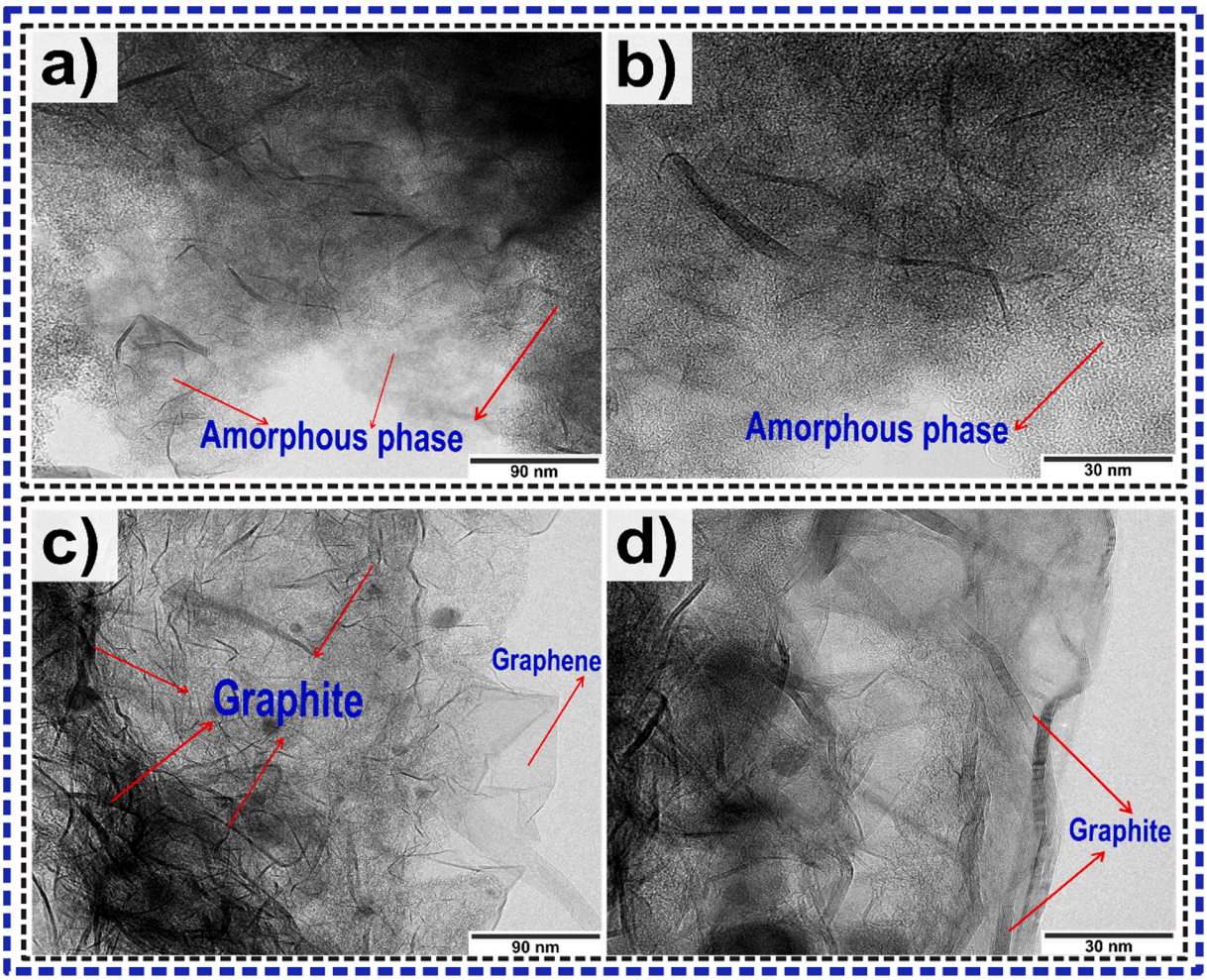

Fig. 2. HRTEM images of CLR (a,b) and BCLR (c,d).

carbon presented an exceptional electrochemical performance. As found in other studies, boron treatment significantly enhanced the formation of crystalline structures (graphite), which leads to better electrochemical performance [36].

To the best of our knowledge, no such approach has been reported in the literature for achieving a high graphitization degree under such a low temperature. The boron-treated highly graphitized carbon from pine logging residue (BCLR) was tested as an anode material in LIBs and electrodes in symmetric supercapacitors. A systematic electrochemical analysis was carried out to demonstrate the effect of boron treatment, the degree of graphitization, and chemical activation on the electrochemical performance of the synthesized material. The BCLR exhibited first charge capacities of 1343 mAh g^{-1} and 886 mAh g^{-1} at 0.1 C and 1 C rates, respectively (1 C = 372 mAh g^{-1}). Conversely, activated carbon without boron-treatment delivered 1482 and 834 mAh g^{-1} at 0.1 C and 1 C rates, respectively. This study establishes a straightforward and cost-effective synthesis method for scaling up carbonaceous electrode materials for LIBs and supercapacitors, facilitated using sustainable precursors and an industrially viable approach.

2. Results and discussion

2.1. Physicochemical characterization of the CLR and BCLR electrode materials

SEM was used to examine the morphology of the CLR and BCLR carbons to gain insights into the impact of the boron-catalyst treatment on the materials' morphological aspects. The SEM images of the CLR (Fig. 1a, 1c) and BCLR (Fig. 1b, 1d) show a clear difference: the boron-treated sample (BCLR) exhibits a much rougher morphology compared to the CLR sample, which has a smoother surface with no cracks or holes (Fig. 1a,c). Additionally, BCLR appears to exhibit a more disordered structure with an agglomeration of smaller particles, indicating the successful modification of the carbon sample's morphology after treatment with the boron catalyst.

The physical features of the CLR and BCLR samples were further evaluated in terms of their porosity and surface area characteristics, which are important properties that significantly influence the electrochemical performance of the electrode materials. Results from the N_2 adsorption/desorption isotherms are presented in the Supplementary Materials (Fig. S1). The N_2 isotherms of the CLR sample showed characteristics of type I with a slight hysteresis, meaning a carbon dominated by microporous structures. The BCLR sample showed a more pronounced hysteresis (from 0.45 to 0.99 of partial pressure), characteristic of type IV, meaning that this carbon has a broader pore size distribution, including micropores, and a larger amount of mesopores compared to the CLR [37]. Such difference between both isotherms could be attributed to the introduction of boron as a catalyst which may cause the collapse of small pores (micropores) and the formation of bigger pores (mesopores), that correspond to the N_2 isotherm curve of BCLR. This transformation is probably responsible for the reduction in the specific surface area of BCLR sample as the contribution of the micropores to the specific surface area (SSA) is larger compared to mesopores.

The CLR and BCLR samples exhibited extremely high SSA of 3141

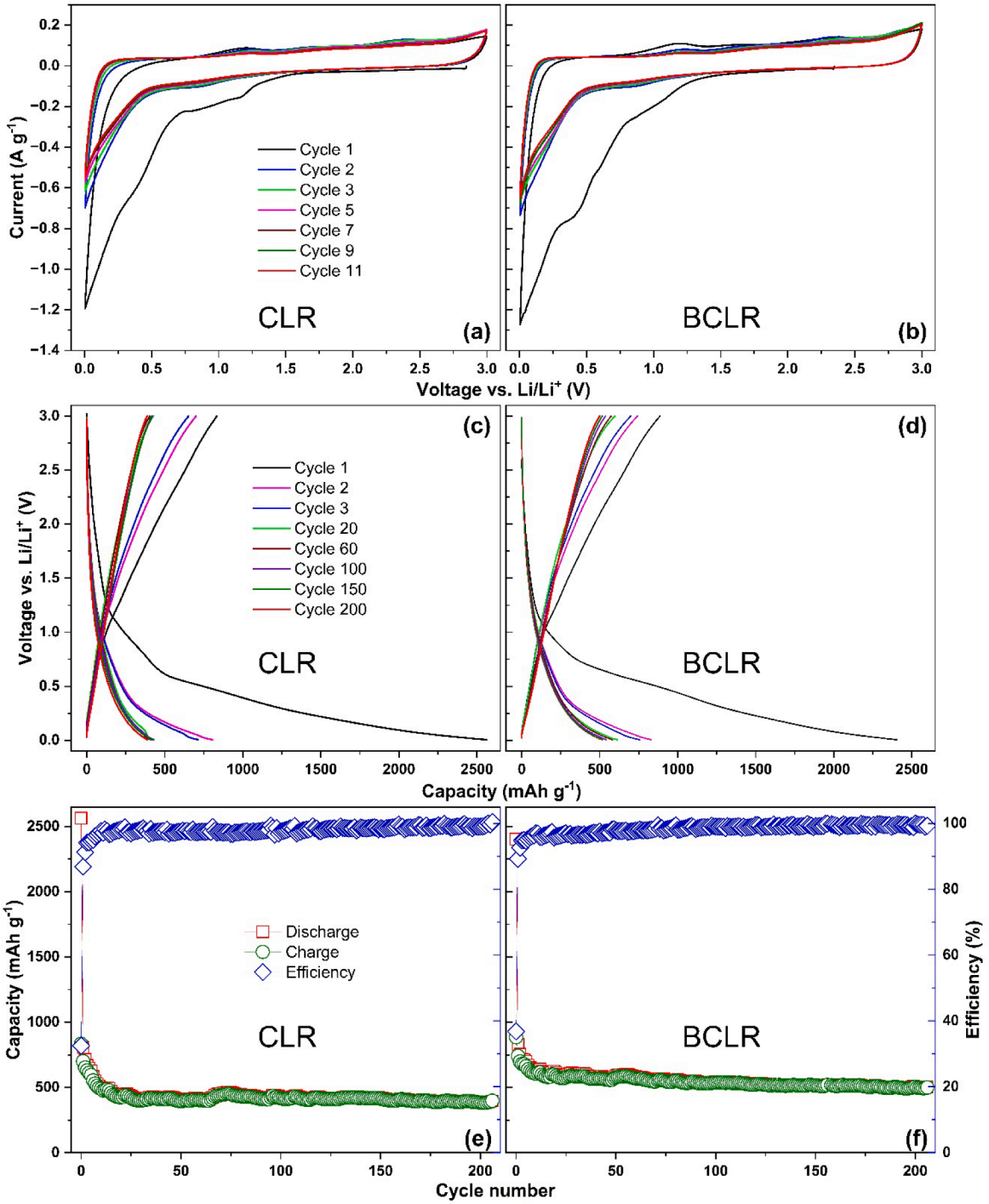

Fig. 3. CV curves of a) CLR and b) BCLR at 0.1 mV s^{-1}scan rate, discharge-charge profiles of c) CLR and d) BCLR and corresponding cycling performance of e) CLR and f) BCLR at 1 C current rate.

and 2645 m^2 g^{-1}, respectively [38]. The synergistic effect of mesopores and micropores leads to a positive impact on the electrochemical performance of the BCLR anode material because more mesopores can provide sufficient space and efficient transport channels for Li^+, thus enabling a faster transport of Li^+ [39]. Therefore, more presence of mesopores in BCLR sample could lead to an enhanced the charge transfer and shortened transport path of Li^+. In addition, bigger pores could also be beneficial for buffering the volume change during the lithiation/delithiation [39].

Raman spectroscopy was employed to evaluate how the boron catalyst affected the carbon structure in terms of the degree of disorder and graphitization of the BCLR (Supplementary Information Fig. S2a, S2b) [38]. The Raman spectra of the LR-based carbons displayed characteristic signatures related to G and D bands centered at ~ 1340 and 1610 cm^{-1}, respectively. However, a remarkable difference in the Raman spectra is observed in the BCLR spectrum (Fig. S2b), with a sharp G' peak (2D peak) at 2680 cm^{-1}. G' peak strongly indicates the presence of graphene structures with a very high degree of stacking. The G band suggests the presence of graphitic structure in the carbon network, while the D band is indicative of structural defects in the carbon lattice. To further evaluate the graphitization process of the boron-treated sample, I_D/I_G was calculated, which indicates graphitization degree. BCLR

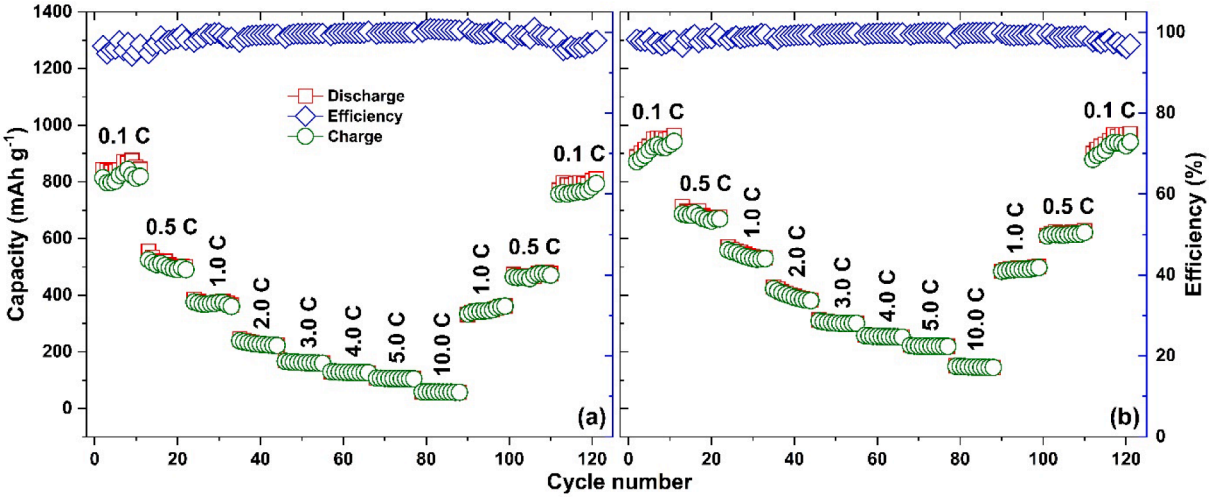

Fig. 4. Rate capability test of a) CLR and b) BCLR samples under various C-rates.

possesses an I_D/I_G value of nearly 0.45 while CLR presented a value of around 0.81. This clearly suggests that the boron, acting as a catalyst, effectively enhanced the graphitization degree of LR carbon under lower graphitization temperatures.

The crystallinity of the CLR and BCLR samples were further evaluated by XRD patterns (Fig. S2c, S2d, Supplementary Information). The pattern shows two evident diffraction peaks that correspond to the (002) and (100) crystal planes of graphitic carbon. The sharp peaks at 26.3° (002) and 44.9° (100) confirm the crystalline structure of both carbons, which suggests the alignment of graphitic carbon layers to form a crystalline turbostratic structure [40]. The XRD spectra (plotted with the same scale for both samples) show that the BCLR has more intense peaks compared to CLR, which can indicate a more crystallographic and better organized aromatic carbon structure in BCLR. These results are in agreement with the Raman spectroscopic data, highlighting the efficient graphitization process of the LR carbon by using boron as a catalyst.

The microstructure of the CLR and BCLR materials was investigated by HRTEM (Fig. 2). Firstly, the TEM images suggest highly porous structures despite of boron catalyst treatment corroborating the BET data. TEM images undoubtedly show that the boron-treated sample (Fig. 2c,d) exhibits a high degree of graphitization, since orderly stacked graphene layers are visible in the images. Much less amorphous phases compared to CLR carbon can be seen (Fig. 2a,b), which although some graphitic structures are observed it has a lot more obvious amorphous phase (disordered/random structures). As previously discussed, boron is an efficient catalyst to promote the graphitization process.

Table S1 shows the elementary composition of the CLR and BCLR materials. The results were obtained from XPS analysis [38]. The results from Table S1 show that both CLR and BCLR are composed of carbon and oxygen. BCLR presented more content of graphitic carbon (C—C bonds) than CLR, corroborating what was observed by TEM and Raman analysis. In BCLR sample, boron content was found in traces (0.25 %, a.*t*-%), confirming the fact that the boron acted as catalyst not as a dopant.

2.2. *Electrochemical performance of the anode materials in LIBs*

The electrochemical performance of CLR and BCLR anodes was evaluated through CV tests and the resulting curves are shown in Fig. 3a, 3b The curves for both samples show typical CV curves for biomass-based carbons [39]. In the first cycle, the broad cathodic peak

Table 1
Comparative electrochemical performance of CLR and BCLR anodes with the biomass carbonaceous materials as LIBs anodes.

Biomass source	Synthesis Method and Morphology	Specific surface area (SBET, $m^2\ g^{-1}$)	Potential (V vs Li^+/Li)	Current rate (C or mA g^{-1})	Initial capacity (Discharge/Charge) (mAh g^{-1})	Capacity retention (mAh g^{-1})/(cycles)	Ref.
Coffee waste grounds	Non-porous carbonaceous materials by mechanochemical dry milling of spent coffee grounds followed by further carbonization at 800 °C	< 10	0.0 – 3.0	100 mA g^{-1}	764/~380	285 ± 5 (100)	[25]
Calotropis gigantea wasteland weed	Activated carbon produced by chemical activation with $CaOCl_2$ in normal atmospheric conditions	–	0.01 – 2.0	1 C	446	137 (100)	[44]
Microalgae	Pyrolysis process in nitrogen flow for 6 h at 900 °C at a heating rate of 10 °C min^{-1}	38	0 - 3.0	1 C	370	355 (500)	[45]
Portobello mushroom	Carbon nanoribbon as free-standing, binder-free, and current collector-free Li-ion battery anodes	19.6	0.01 – 3.0	50 mA g^{-1}	771.3/280	~260 (700)	[46]
Commercial Loofah	Treated with KOH solution (5 M) and pyrolysed at 1000 °C for 2 h.	270	0.01 – 3.0	100 mA g^{-1}	250	225 (400)	[47]
Hazelnut shells	Hydrothermal carbonization plus pyrolysis at 600 °C for 2 h with KOH activation	150	0.05 – 2.0	1 C	511	307 (100)	[48]
Bagasse	N,P co-doped bagasse-based sheet-like mesoporous carbon by hydrothermal activation method	1307.21 to 2118.59	0.01 – 3.0	100 mA g^{-1}	2347.56/ 1186.59	816.36 (50)	[49]
Spongy pomelo peels	Carbonized at 900 °C for 3 h with a heating ramp of 2 °C min^{-1}.	114	0.0 – 2.0	90 mA g^{-1}	450	452 (200)	[50]
CLR	**Pyrolysed at 500 °C and further activated with KOH (1:6) at 900 °C for 1 h.**	**3141**	**0.005 – 3.0**	**1 C (372 mA g^{-1})**	**~834**	**386 (200)**	**This work**
BCLR	**Pyrolysed at 500 °C with 30 wt. % of pure boron, and further activated with KOH (1:6) at 900 °C for 1 h**	**2645**	**0.005 – 3.0**	**1 C (372 mA g^{-1})**	**~886**	**505 (200)**	**This work**

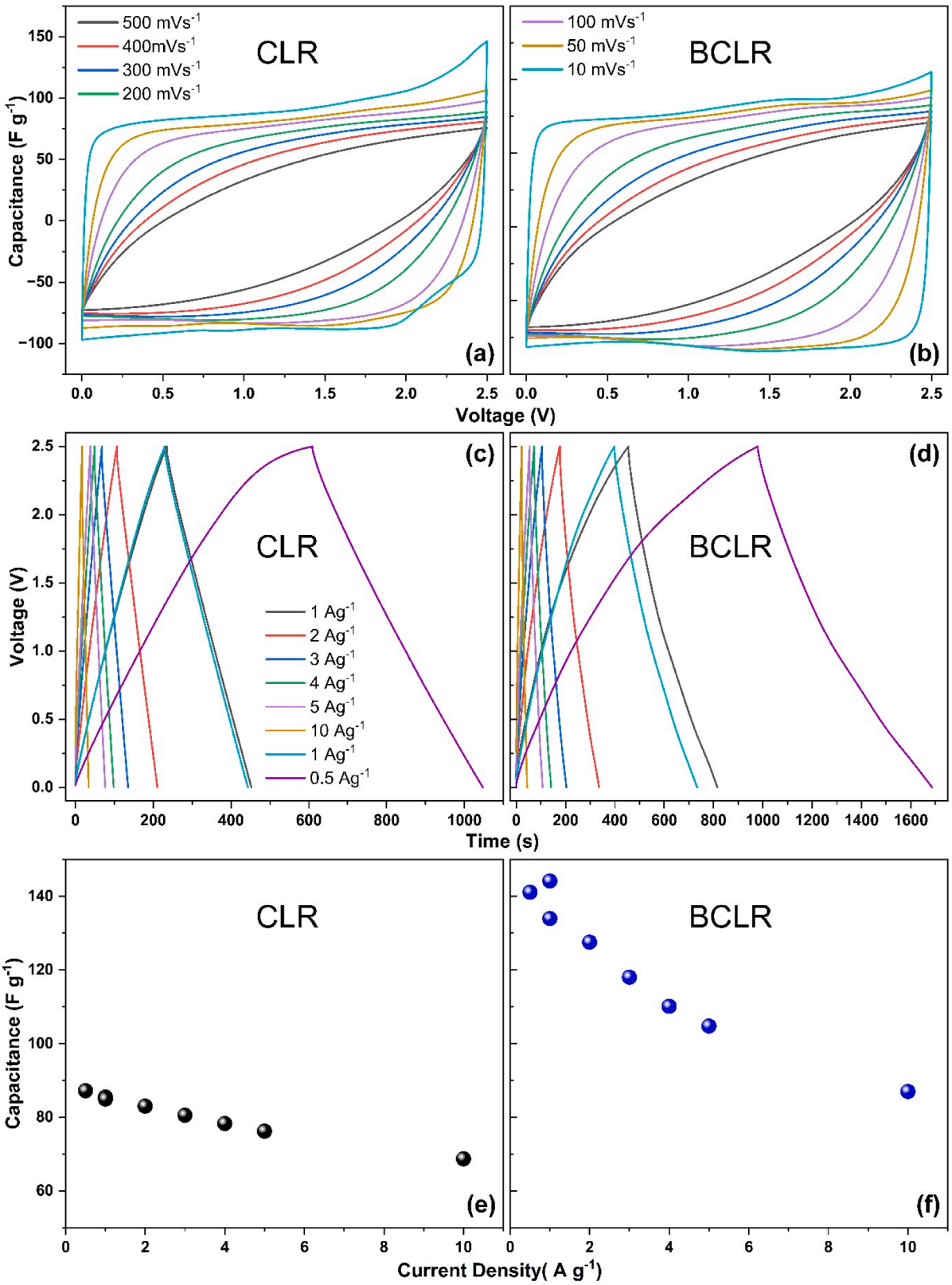

Fig. 5. CV curves of a) CLR and b) BCLR at various scan rates, GCD curves for c) CLR and d) BCLR at different current densities, and discharge capacitances of e) CLR and f) BCLR at different current densities.

between 1.5 and 0.1 V can be related to the irreversible solid electrolyte interface (SEI) film formation. This peak is not observed in the subsequent cycles, suggesting that the SEI formation predominantly occurred in the first cycle. The irreversible SEI formation in the first cycle is due to the decomposition of the electrolyte that traps Li-ions permanently onto surfaces of the carbon materials, leading to a significant drop in the capacity (Fig. 3c, 3d) and resulted in an extremely low first cycle Coulombic efficiency (CE). From the second cycle onwards a non-zero

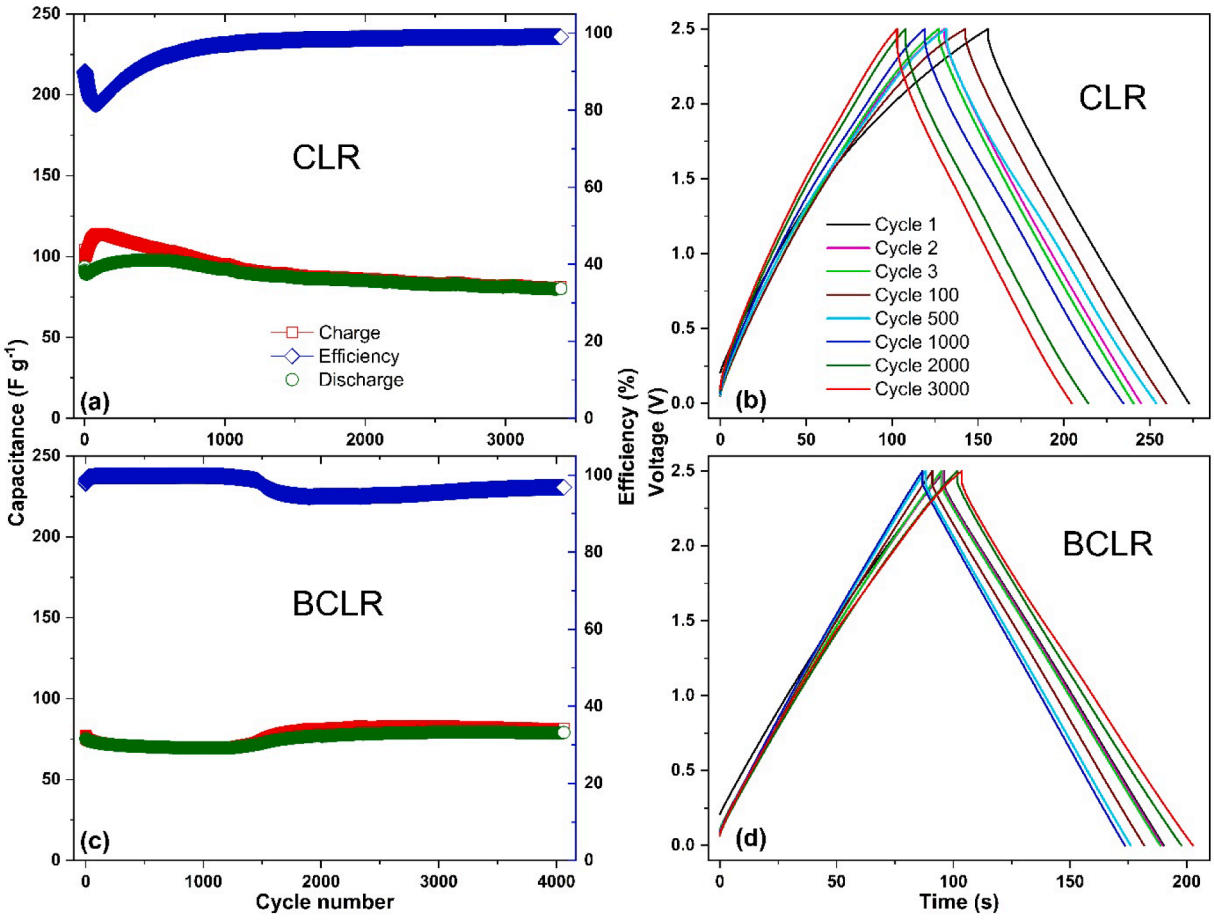

Fig. 6. Cycling stability performance of CLR (a,b) and BCLR (c,d) electrodes at a current density of 2 A g^{-1}.

reduction current notice from 3.0 to 0.5 V originates mainly from electrochemical absorption of Li-ions whilst the storage mechanism turns to intercalation between 0.5 and 0.005 V [41–43]. The CV profiles show non-zero oxidation current throughout the anodic scan, in the charging process, which refers to the electrochemical desorption of Li-ions from CLR and BCLR anodes [41–43]. At 1 C rate, CLR electrode exhibited first charge capacity retention of 834 mAh g^{-1} that retained 46 % (386 mAh g^{-1}) at the end of 200th cycle, whereas BCLR showed a respective capacity of 886 mAh g^{-1} and a higher retention of 57 % (505 mAh g^{-1}) (Fig. 3e, 3f). Nonetheless, both the anodes showed stable capacity values from 20th cycle onwards as seen in Fig. 3e and Fig. 3f. The CE was improved, reaching 88 % for both carbons during the 2nd cycle that further attained 99 % throughout the cycling after initial few cycles, indicating good cycling stability of the LR carbon anodes. The electrochemical metrics of the CLR and BCLR anodes were further improved to cycling performance at 0.1 C rate (see supplementary materials Fig. S3), exhibited a capacity of 849 mAh g^{-1} and 909 mAh g^{-1} at the end of 46 cycles corresponding to the capacities retention of 57 and 68 %, respectively. The continuous sloping capacity curves observed in Fig. 3e, Fig. 3f, and Fig. S3 indicate that the electrochemical absorption-desorption of Li ions is the dominant storage mechanism in all cases, regardless of the applied current densities.

Fig. 4 exhibits the results of rate capability performance for CLR and BCLR anodes at different current densities (e.g., 0.1 C, 0.5 C, 1 C, 2 C, 3 C, 4 C, 5 C, 10 C). As expected, the cell capacity decreased with increasing C-rates. However, both electrodes exhibited remarkable recovery of their initial capacity when the C-rate was returned to the initial value (i.e., 0.1 C), giving reversible capacity values of 810 and 941 mA h g^{-1} for CLR and BCLR, respectively. Even at very high current rate of 10 C, CLR and BCLR delivered charge capacities of 58 and 146 mA h g^{-1}, respectively which are impractical in the case of commercial graphite anode [41–43]. Such results strongly suggest an outstanding capacity reversibility for both materials. The higher capacity of BCLR samples at all the C-rates confirms that the boron catalyst is an effective and easy strategy to produce high-performance graphitized anodes from biomass using low temperature for suitable applications such as anodes in LIBs.

The electrochemical performances of CLR and BCLR anodes are compared to those in many reported works in the literature (Table 1). The graphitized carbon (BCLR) exhibited an extremely high SSA value (2645 m^2 g^{-1}) compared to the others. We emphasize that graphitized carbon outperforms most of the anodes reported in the literature, and it can be considered a benchmark against the state-of-the-art biomass LIB anodes, as detailed in Table 1.

2.3. *Electrochemical characterization of the CLR and BCLR electrode in supercapacitors*

The impact of boron-assisted graphitization on the electrochemical performance of a symmetric SCs system was investigated using CV under different scan rates. Fig. 5a, 5b summarizes the CV test curves for CLR and BCLR electrodes recorded with 10–500 mV s^{-1} scan rates. The data show a quasi-rectangular shape in the response acquired at lower scan rates of 10–100 mV s^{-1} is observed for both materials, which indicates that both electrodes possess a reversible charge and discharge mechanism and good performance of electric double-layer capacitance (EDLC) contribution [51,52]. The XPS analysis of both carbons is given in a previous publication [36], and the elemental composition is reproduced in Supplementary Materials, Table S1. The pseudocapacitance provided by oxygen functional groups (C—O-, *C = O*) as well as

Table 2
Gravimetric capacitance of selected biomass-carbon-based non-aqueous supercapacitors.

Electrode material	Capacitance ($F\ g^{-1}$)	Electrolyte	Current ($A\ g^{-1}$)	Ref.
Porous graphene nanosheets	128.2	2.0 M $EMIMBF_4$/ acetonitrile	1.0	[58]
Porous carbon material (CBW)	80	$[BMIM]BF_4$/AN	2.0	[51]
3D hierarchical porous carbon from fulvic acid biomass	~124	$EMIMBF_4$	1.0	[59]
N and S co-doped activated carbon	70	EMIMFSI	1.0	[60]
Sulfur-doped carbon nanotubes	27	1 M $TEABF_4$/ AN	–	[57]
Pine cone activated carbon	118.01	1 M TEA-BF_4	1	[61]
Spruce cone activated carbon	122.53	1 M TEA-BF_4	1	
Larch cone activated carbon	105.61	1 M TEA-BF_4	1	
Birch wood activated carbon	105	1 M TEA-BF_4	1	[62]
Spent mushroom substrate activated carbon	87	1 M TEA-BF_4	1	
Pine cone-activated carbon sprayed-coated	105	1 M TEA-BF_4	0.5	[63]
Pine cone-activated carbon blade-coated	93	1 M TEA-BF_4	0.5	
Pine cone-activated carbon pelletized	90	1 M TEA-BF_4	0.5	
CLR	**87**	**$EMIMBF_4$/ acetonitrile**	**1.0**	**This work**
BCLR	**144**	**$EMIMBF_4$/ acetonitrile**	**1.0**	**This work**

intercalation/de-intercalation of anions in graphitic structures could be another plausible reason behind the rectangular shapes. In general, the ionic transportation phenomenon is diffusion-dominant that results in rectangular-shaped CV features [51,52]. At higher scan rates, an obvious change in the CV curve is observed. It acquires a more prolate shape as seen in Fig. 5a-b due to the ionic transport mechanism change to surface dominant, which is otherwise also known as the C-rate effect [51,52]. At high scan rates or C-rates, part of the electroactive process becomes inactive, thus leading to prolate shapes, and those inactive reactions can be reactivated at low C-rates, switching the shapes back to rectangular [52,53], which could be due to the pseudocapacitance provided by oxygen functional groups (C—O, *C = O*, OH, COOH) as well as intercalation/de-intercalation of anions in graphitic structure. The electrochemical performance of the materials was further evaluated through GCD curves (Fig. 5c, 5d). As can be seen, GCD curves at high current rates exhibited a well-symmetrical triangle, which discloses the reversible ion adsorption/desorption process and efficient ionic transfer at the electrode/electrolyte interfaces, which further highlights the EDLC characteristics of the LR-carbon materials. Fig. 5e-f displays the specific capacitance at different current densities, and the maximum discharge capacitance was achieved by the BCLR electrode for all current densities, with the highest value being 141 $F\ g^{-1}$ at 0.1 $A\ g^{-1}$ for BCLR. Sun et al., [54] reported that Graphitic porous carbon possesses structural merits for SCs application because of its high BET surface area, well-developed graphitic carbon lattice, and high packing density. The specific capacitance of the BCLR was higher than that of the CLR due to the synergistic effect of its graphitic and porous structure within the carbon network. Such structures can facilitate electron transfer and charge storage because the electrons can be efficiently delivered into the pore surface along the graphitic carbon fringes, while the porous structures surrounded by the graphitized framework facilitates surface as well as space charge storage.

The electrochemical stability of the CLR and BCLR-based SCs were evaluated by successive GCD assays in which a current of 2.0 A/g was applied, and their results are summarized in Fig. 6**a-d**. BCLR electrode showed high retention in the capacitance with almost no loss over 4000 cycles, while CLR exhibited a gradual capacitance decay trend within 3500 cycles (Fig. 6**a,c**). The degradation in the cycling performance of CLR samples may be attributed to its predominantly amorphous carbon framework, which exhibits predominantly lower electrical conductivity than the graphitic structure. Both samples indicate an electrical double-layer behavior (Fig. 6b,d), and the better electrochemical performances of BCLR compared to CLR could also be explained by the optimal balance between graphitization, pore structure richer in mesopores, and surface chemistry in BCLR, which provides high conductivity and sufficient active sites for ion storage [55], besides BCLR has a more mesoporous structure which facilitates the ions diffusion because they can accommodate a considerable number of solvated electrolyte ions, which serve as ion storage reservoirs [55], and thus, improving the capacitance by favoring a fast double-layer charging and discharging process [56].

Table 2 compares the gravimetric capacitance performance of CLR and BCLR-based SCs with other similar devices reported in recent literature. The data displayed in Table 2 confirms the potential of the graphitic material (BCLR) as the potential electrode for SCs since it exhibited a very good performance compared to the ones shown in Table 2. For instance, the SCs based on sulfur-doped carbon nanotubes [57], displayed a low capacitance of 27 $F\ g^{-1}$ at 1 $A\ g^{-1}$, moreover the carbon nanotubes are much more expensive and its synthesis is highly complex. The SCs based on graphene nanosheets exhibited a capacitance of 128 $F\ g^{-1}$ at 1 $A\ g^{-1}$, and graphene is an expensive material as well. Thus, it can be concluded that BCLR material exhibits highly promising performance on SCs application, as also indicated in LIBs, suggesting that the BCLR could be employed as an efficient electrode for SCs and LIBs.

3. Conclusions

In summary, pine tree logging residues, a highly abundant and inexpensive biomass feedstock in northern countries, were thermochemically transformed into highly porous graphitic carbon using pure boron as an efficient catalyst to enhance the graphitization process at low temperatures. The boron-treated sample (BCLR) exhibited a lower specific surface area (2645 $m^2\ g^{-1}$) than that of non-boron treated (CLR, 3141 $m^2\ g^{-1}$); however, the boron-treated sample exhibited far more graphitic layers in its structure, highlighting its high graphitization degree. The high graphitization degree alongside its well-developed porosity helped to deliver a much higher specific capacity of 505 mAh g^{-1} at 1 C for the BCLR anode at the end of 200 cycles whilst the respective capacity for CLR was 386 mAh g^{-1}. When applied as supercapacitor electrodes, the BCLR delivered a much higher specific capacitance of 144 $F\ g^{-1}$ at 1 $A\ g^{-1}$ compared to non-boron treated (87 $F\ g^{-1}$ at 1 $A\ g^{-1}$). Furthermore, BCLR exhibited excellent cycle stability (capacitance retention of 98 % over 4000 cycles). The physicochemical and electrochemical results confirm that graphitized porous carbon derived from logging residues is a promising candidate for high-rate electrochemical performance as electrodes in LIBs and SCs applications.

Appendix. Supplementary materials: The materials and methods are found in the supplementary information.

Funding information

This work was supported by the financial support of the EU/Interreg Aurora (Project GreenBattery, grant no 20,357,574), EU/Interreg Aurora (Project: Nature Refines, grant no. 20361711), the Swedish Research Council FORMAS (grant no. 2021–00877), and Kempestiftelserna (grant no. JCSMK23–0145). AG, SSP, and MT thank

Bio4Energy - a Strategic Research Environment appointed by the Swedish government and the Swedish University of Agricultural Sciences. Dr. Glaydson dos Simoes Reis gratefully acknowledges financial support from the Research Council of Finland (Academy Research Fellows 2024, Project: Bio-Adsorb&Energy, grant No. 361583). The authors also acknowledge Business Finland for research funding 2021–2024, the University of Oulu (BATCircle2.0, No. 44612/31/2020).

CRediT authorship contribution statement

Sruthy E S: Writing – original draft, Validation, Software, Methodology, Investigation, Formal analysis, Conceptualization. **Alejandro Grimm:** Writing – review & editing, Methodology, Formal analysis. **Menestreau Paul:** Writing – review & editing, Methodology, Investigation, Formal analysis. **Christie Thomas Cherian:** Writing – review & editing, Visualization, Validation, Funding acquisition, Data curation. **Mikael Thyrel:** Project administration, Funding acquisition. **Palanivel Molaiyan:** Writing – review & editing, Validation. **Ulla Lassi:** Writing – review & editing, Project administration, Data curation. **Shaikshavali Petnikota:** Writing – review & editing, Visualization, Investigation, Data curation, Conceptualization. **Glaydson Simões Dos Reis:** Writing – review & editing, Writing – original draft, Methodology, Formal analysis, Data curation, Conceptualization.

Declaration of competing interest

The authors declare the following financial interests/personal relationships which may be considered as potential competing interests: Glaydson Simoes dos Reis reports financial support was provided by Swedish University of Agricultural Sciences. If there are other authors, they declare that they have no known competing financial interests or personal relationships that could have appeared to influence the work reported in this paper.

Acknowledgments

This work was supported by the financial support of the EU/Interreg Aurora (Project GreenBattery, grant no. 20357574), EU/Interreg Aurora (Project: Nature Refines, grant no. 20361711), the Swedish Research Council FORMAS (grant no. 2021–00877), and Kempestiftelserna (grant no. JCSMK23–0145). AG, SSP, and MT thank Bio4Energy - a Strategic Research Environment appointed by the Swedish government and the Swedish University of Agricultural Sciences. Dr. Glaydson dos Simoes Reis gratefully acknowledges financial support from the Research Council of Finland (Academy Research Fellows 2024, Project: Bio-Adsorb&Energy, grant No. 361583).

Supplementary materials

Supplementary material associated with this article can be found, in the online version, at doi:10.1016/j.ceja.2025.100762.

Data availability

Data will be made available on request.

References

[1] Q. Qin, J. Wang, Z. Tang, Y. Jiang, L. Wang, Mesoporous activated carbon for supercapacitors derived from coconut fiber by combining H3PO4-assisted hydrothermal pretreatment with KOH activation, Ind. Crops Prod. 208 (2024) 117878, https://doi.org/10.1016/j.indcrop.2023.117878.

[2] A.K. Mondal, K. Kretschmer, Y. Zhao, H. Liu, C. Wang, B. Sun, G. Wang, Nitrogen-Doped Porous Carbon Nanosheets from Eco-Friendly Eucalyptus Leaves as High Performance Electrode Materials for Supercapacitors and Lithium Ion Batteries, Chem. – A Eur, J. 23 (2017) 3683–3690, https://doi.org/10.1002/chem.201605019.

[3] H. Cavers, P. Molaiyan, M. Abdollahifar, U. Lassi, A. Kwade, Perspectives on Improving the Safety and Sustainability of High Voltage Lithium-Ion Batteries Through the Electrolyte and Separator Region, Adv. Energy Mater. 12 (2022) 2200147, https://doi.org/10.1002/aenm.202200147.

[4] C. Yuan, H. Xu, S.A. El-khodary, G. Ni, S. Esakkimuthu, S. Zhong, S. Wang, Recent advances and challenges in biomass-derived carbon materials for supercapacitors: a review, Fuel 362 (2024) 130795, https://doi.org/10.1016/j.fuel.2023.130795.

[5] G.S. dos Reis, H.P. de Oliveira, I.C.M. Candido, A.L. Freire, P. Molaiyan, G.L. Dotto, A. Grimm, J.-P. Mikkola, Supercapacitors and triboelectric nanogenerators based on electrodes of greener iron nanoparticles/carbon nanotubes composites, Sci. Rep. 14 (2024) 11555, https://doi.org/10.1038/s41598-024-61173-5.

[6] S.K. Saju, S. Chattopadhyay, J. Xu, S. Alhashim, A. Pramanik, P.M. Ajayan, Hard carbon anode for lithium-, sodium-, and potassium-ion batteries: advancement and future perspective, Cell Reports Phys. Sci. 5 (2024) 101851, https://doi.org/10.1016/j.xcrp.2024.101851.

[7] X. Zhou, F. Chen, T. Bai, B. Long, Q. Liao, Y. Ren, J. Yang, Interconnected highly graphitic carbon nanosheets derived from wheat stalk as high performance anode materials for lithium ion batteries, Green Chem. 18 (2016) 2078–2088. https://doi.org/10.1039/C5GC02122G.

[8] P. Molaiyan, B. Boz, G.S. dos Reis, R. Sliz, S. Wang, M. Borsari, U. Lassi, A. Paolella, Paving the path toward silicon as anode material for future solid-state batteries, ETransportation 23 (2025) 100391, https://doi.org/10.1016/j.etran.2024.100391.

[9] G. Liu, Y. Zhao, J. Li, T. Zhang, M. Yang, D. Guo, N. Wu, K. Wu, X. Liu, Hierarchical N/O co-doped hard carbon derived from waste saccharomyces cerevisiae for lithium storage, J. Electroanal. Chem. 911 (2022) 116226, https://doi.org/10.1016/j.jelechem.2022.116226.

[10] M. Ullah, M.M. Hasan, R. Roslan, R. Jose, I.I. Misnon, Sustainable graphitic carbon derived from oil palm frond biomass for supercapacitor application: effect of redox additive and artificial neural network-based modeling approach, J. Electroanal. Chem. 971 (2024) 118570, https://doi.org/10.1016/j.jelechem.2024.118570.

[11] P. Molaiyan, S. Bhattacharyya, G.S. dos Reis, R. Sliz, A. Paolella, U. Lassi, Towards greener batteries: sustainable components and materials for next-generation batteries, Green. Chem. 26 (2024) 7508–7531, https://doi.org/10.1039/d3gc05027k.

[12] P. Molaiyan, G.S. Dos Reis, D. Karuppiah, C.M. Subramaniyam, F. García-Alvarado, U. Lassi, Recent Progress in Biomass-Derived Carbon Materials for Li-Ion and Na-Ion Batteries—A Review, Batteries. (Basel) 9 (2023), https://doi.org/10.3390/batteries9020116.

[13] R.M. Lima, G.S. dos Reis, M. Thyrel, J.J. Alcaraz-Espinoza, S.H. Larsson, H.P. de Oliveira, Facile Synthesis of Sustainable Biomass-Derived Porous Biochars as Promising Electrode Materials for High-Performance Supercapacitor Applications, Nanomaterials 12 (2022), https://doi.org/10.3390/nano12050866.

[14] R.M. Lima, G.S. dos Reis, U. Lassi, E.C. Lima, G.L. Dotto, H.P. de Oliveira, Sustainable Supercapacitors Based on Polypyrrole-Doped Activated Biochar from Wood Waste Electrodes, C. (Basel) 9 (2023), https://doi.org/10.3390/c9020059.

[15] G.S. dos Reis, P. Molaiyan, C.M. Subramaniyam, F. García-Alvarado, A. Paolella, H. P. de Oliveira, U. Lassi, Biomass-derived carbon–silicon composites (C@Si) as anodes for lithium-ion and sodium-ion batteries: a promising strategy towards long-term cycling stability: a mini review, Electrochem. Commun. 153 (2023) 107536, https://doi.org/10.1016/j.elecom.2023.107536.

[16] R.R. Gaddam, D. Yang, R. Narayan, K. Raju, N.A. Kumar, X.S. Zhao, Biomass derived carbon nanoparticle as anodes for high performance sodium and lithium ion batteries, Nano Energy 26 (2016) 346–352, https://doi.org/10.1016/j.nanoen.2016.05.047.

[17] G.S. Dos Reis, S. Tuomikoski, D. Bergna, S. Larsson, M. Thyrel, H.P. de Oliveira, P. Molaiyan, U. Lassi, Chapter 20 - Waste biomass conversion to energy storage material, in: A. Sarkar, U.B.T.-P. of B.W. Lassi (Eds.), Elsevier, 2024: pp. 285–304. https://doi.org/10.1016/B978-0-323-95179-1.00020-7.

[18] L. Wang, Z. Schnepp, M.M. Titirici, Rice husk-derived carbon anodes for lithium ion batteries, J. Mater. Chem. A 1 (2013) 5269–5273, https://doi.org/10.1039/C3TA10650K.

[19] Y. Ju, J.A. Tang, K. Zhu, Y. Meng, C. Wang, G. Chen, Y. Wei, Y. Gao, SiOx/C composite from rice husks as an anode material for lithium-ion batteries, Electrochim. Acta 191 (2016) 411–416, https://doi.org/10.1016/j.electacta.2016.01.095.

[20] G.T.-K. Fey, D.C. Lee, Y.Y. Lin, T.P. Kumar, High-capacity disordered carbons derived from peanut shells as lithium-intercalating anode materials, Synth. Met. 139 (2003) 71–80, https://doi.org/10.1016/S0379-6779(03)00082-1.

[21] G. Xu, J. Han, B. Ding, P. Nie, J. Pan, H. Dou, H. Li, X. Zhang, Biomass-derived porous carbon materials with sulfur and nitrogen dual-doping for energy storage, Green. Chem. 17 (2015) 1668–1674, https://doi.org/10.1039/C4GC02185A.

[22] W.E. Tenhaeff, O. Rios, K. More, M.A. McGuire, Highly Robust Lithium Ion Battery Anodes from Lignin: an Abundant, Renewable, and Low-Cost Material, Adv. Funct. Mater. 24 (2014) 86–94, https://doi.org/10.1002/adfm.201301420.

[23] A. Caballero, L. Hernán, J. Morales, Limitations of Disordered Carbons Obtained from Biomass as Anodes for Real Lithium-Ion Batteries, ChemSusChem. 4 (2011) 658–663, https://doi.org/10.1002/cssc.201000398.

[24] Y. Mao, H. Duan, B. Xu, L. Zhang, Y. Hu, C. Zhao, Z. Wang, L. Chen, Y. Yang, Lithium storage in nitrogen-rich mesoporous carbon materials, Energy Environ. Sci. 5 (2012) 7950–7955, https://doi.org/10.1039/C2EE21817H.

[25] F. Luna-Lama, D. Rodríguez-Padrón, A.R. Puente-Santiago, M.J. Muñoz-Batista, A. Caballero, A.M. Balu, A.A. Romero, R. Luque, Non-porous carbonaceous materials derived from coffee waste grounds as highly sustainable anodes for lithium-ion batteries, J. Clean. Prod. 207 (2019) 411–417, https://doi.org/10.1016/j.jclepro.2018.10.024.

[26] L. Li, C. Fan, Y. Tang, B. Zeng, Synthesis and characterization of PVDF-coated cotton-derived hard carbon for anode of Li-ion batteries, Int. J. Energy Res. 43 (2019) 4987–4994, https://doi.org/10.1002/er.4593.
[27] D. Feng, Y. Li, X. Qin, L. Zheng, B. Guo, W. Dai, N. Song, L. Liu, Y. Xu, Z. Tang, T. Gao, Biomass derived porous carbon anode materials for lithium-ion batteries with high electrochemical performance, Int. J. Electrochem. Sci. 19 (2024) 100488, https://doi.org/10.1016/j.ijoes.2024.100488.
[28] J.G. Kim, F. Liu, C.-W. Lee, Y.-S. Lee, J.S. Im, Boron-doped carbon prepared from PFO as a lithium-ion battery anode, Solid. State Sci. 34 (2014) 38–42, https://doi.org/10.1016/j.solidstatesciences.2014.05.005.
[29] J. Hoekstra, A.M. Beale, F. Soulimani, M. Versluijs-Helder, J.W. Geus, L. W. Jenneskens, Base Metal Catalyzed Graphitization of Cellulose: a Combined Raman Spectroscopy, Temperature-Dependent X-ray Diffraction and High-Resolution Transmission Electron Microscopy Study, J. Phys. Chem. C 119 (2015) 10653–10661, https://doi.org/10.1021/acs.jpcc.5b00477.
[30] S. Xia, H. Yang, W. Lu, N. Cai, H. Xiao, X. Chen, Y. Chen, X. Wang, S. Wang, P. Wu, H. Chen, Fe–Co based synergistic catalytic graphitization of biomass: influence of the catalyst type and the pyrolytic temperature, Energy 239 (2022) 122262, https://doi.org/10.1016/j.energy.2021.122262.
[31] L. Gai, J. Li, Q. Wang, R. Tian, K. Li, Evolution of biomass to porous graphite carbon by catalytic graphitization, J. Environ. Chem. Eng. 9 (2021) 106678, https://doi.org/10.1016/j.jece.2021.106678.
[32] Y. Nakayasu, Y. Goto, Y. Katsuyama, T. Itoh, M. Watanabe, Highly crystalline graphite-like carbon from wood via low-temperature catalytic graphitization, Carbon Trends 8 (2022) 100190, https://doi.org/10.1016/j.cartre.2022.100190.
[33] S. Lee, S.Y. Cho, Y.S. Chung, Y.C. Choi, S. Lee, High electrical and thermal conductivities of a PAN-based carbon fiber via boron-assisted catalytic graphitization, Carbon N. Y. 199 (2022) 70–79, https://doi.org/10.1016/j.carbon.2022.07.068.
[34] J. Wang, S. Kaskel, KOH activation of carbon-based materials for energy storage, J. Mater. Chem. 22 (2012) 23710–23725, https://doi.org/10.1039/C2JM34066F.
[35] C. Hernández-Rentero, V. Marangon, M. Olivares-Marín, V. Gómez-Serrano, Á. Caballero, J. Morales, J. Hassoun, Alternative lithium-ion battery using biomass-derived carbons as environmentally sustainable anode, J. Colloid Interface Sci. 573 (2020) 396–408, https://doi.org/10.1016/j.jcis.2020.03.092.
[36] C. Wang, F. Luo, H. Lu, X. Rong, B. Liu, G. Chu, Y. Sun, B. Quan, J. Zheng, J. Li, C. Gu, X. Qiu, H. Li, L. Chen, A Well-Defined Silicon Nanocone–Carbon Structure for Demonstrating Exclusive Influences of Carbon Coating on Silicon Anode of Lithium-Ion Batteries, ACS Appl. Mater. Interfaces 9 (2017) 2806–2814, https://doi.org/10.1021/acsami.6b13028.
[37] M. Thommes, K. Kaneko, A.V. Neimark, J.P. Olivier, F. Rodriguez-Reinoso, J. Rouquerol, K.S.W. Sing, Physisorption of gases, with special reference to the evaluation of surface area and pore size distribution (IUPAC Technical Report), 87 (2015) 1051–1069. doi:10.1515/pac-2014-1117.
[38] A. Grimm, S. Conrad, F.G. Gentili, J.-P. Mikkola, T. Hu, U. Lassi, L.F.O. Silva, E. C. Lima, G.S. dos Reis, Highly efficient boron/sulfur-modified activated biochar for removal of reactive dyes from water: kinetics, isotherms, thermodynamics, and regeneration studies, Colloids Surfaces A Physicochem. Eng. Asp. 713 (2025) 136486, https://doi.org/10.1016/j.colsurfa.2025.136486.
[39] G. Simões dos Reis, C. Mayandi Subramaniyam, A.D. Cárdenas, S.H. Larsson, M. Thyrel, U. Lassi, F. García-Alvarado, Facile Synthesis of Sustainable Activated Biochars with Different Pore Structures as Efficient Additive-Carbon-Free Anodes for Lithium- and Sodium-Ion Batteries, ACS. Omega 7 (2022) 42570–42581, https://doi.org/10.1021/acsomega.2c06054.
[40] Y. Li, B. Xing, X. Wang, K. Wang, L. Zhu, S. Wang, Nitrogen-Doped Hierarchical Porous Biochar Derived from Corn Stalks for Phenol-Enhanced Adsorption, Energy & Fuels 33 (2019) 12459–12468, https://doi.org/10.1021/acs.energyfuels.9b02924.
[41] S. Petnikota, N.K. Rotte, V.V.S.S. Srikanth, B.S.R. Kota, M.V. Reddy, K.P. Loh, B.V. R. Chowdari, Electrochemical studies of few-layered graphene as an anode material for Li ion batteries, J. Solid State Electrochem. 18 (2014) 941–949, https://doi.org/10.1007/s10008-013-2338-2.
[42] S. Petnikota, N.K. Rotte, M.V. Reddy, V.V.S.S. Srikanth, B.V.R. Chowdari, MgO-Decorated Few-Layered Graphene as an Anode for Li-Ion Batteries, ACS Appl. Mater. Interfaces 7 (2015) 2301–2309, https://doi.org/10.1021/am5064712.
[43] H. Maseed, S. Petnikota, V.V.S.S. Srikanth, N.K. Rotte, M. Srinivasan, F. Bonaccorso, V. Pellegrini, M.V. Reddy, A new insight into Li-staging, in-situ electrochemical exfoliation, and superior Li storage characteristics of highly crystalline few-layered graphene, J. Energy Storage 41 (2021) 102908, https://doi.org/10.1016/j.est.2021.102908.
[44] A. Sahu, A. Kumar, L. Dashairya, P. Saha, S.K. Bhuyan, S. Sen, S.C. Mishra, Performance of wasteland biomass Calotropis gigantea derived activated carbon as Lithium-ion battery anode, Diam. Relat. Mater. 136 (2023) 110053, https://doi.org/10.1016/j.diamond.2023.110053.
[45] H. Ru, N. Bai, K. Xiang, W. Zhou, H. Chen, X.S. Zhao, Porous carbons derived from microalgae with enhanced electrochemical performance for lithium-ion batteries, Electrochim. Acta 194 (2016) 10–16, https://doi.org/10.1016/j.electacta.2016.02.083.
[46] B. Campbell, R. Ionescu, Z. Favors, C.S. Ozkan, M. Ozkan, Binderless Bio-Derived, Hierarchically Porous Carbon Anodes for Li-ion Batteries, Sci. Rep. 5 (2015) 14575, https://doi.org/10.1038/srep14575.
[47] Z. Wu, L. Wang, J. Huang, J. Zou, S. Chen, H. Cheng, C. Jiang, P. Gao, X. Niu, Loofah-derived carbon as an anode material for potassium ion and lithium ion batteries, Electrochim. Acta 306 (2019) 446–453, https://doi.org/10.1016/j.electacta.2019.03.165.
[48] E. Unur, S. Brutti, S. Panero, B. Scrosati, Nanoporous carbons from hydrothermally treated biomass as anode materials for lithium ion batteries, Microporous Mesoporous Mater 174 (2013) 25–33, https://doi.org/10.1016/j.micromeso.2013.02.032.
[49] S. Zheng, Y. Luo, K. Zhang, H. Liu, G. Hu, A. Qin, Nitrogen and phosphorus co-doped mesoporous carbon nanosheets derived from bagasse for lithium-ion batteries, Mater. Lett. 290 (2021) 129459, https://doi.org/10.1016/j.matlet.2021.129459.
[50] X. Sun, X. Wang, N. Feng, L. Qiao, X. Li, D. He, A new carbonaceous material derived from biomass source peels as an improved anode for lithium ion batteries, J. Anal. Appl. Pyrolysis 100 (2013) 181–185, https://doi.org/10.1016/j.jaap.2012.12.016.
[51] M. Paul, A. Grimm, G. Simões Dos Reis, G. Manavalan, S. ES, M. Thyrel, S. Petnikota, Activated Carbon from Birch Wood as an Electrode Material for Aluminum Batteries and Supercapacitors, ChemElectroChem. 12 (2025) e202400549, https://doi.org/10.1002/celc.202400549.
[52] S. Petnikota, V.V.S.S. Srikanth, J.J. Toh, M. Srinivasan, C.V.R. Bobba, S. Adams, M. V. Reddy, Electrochemistry-related aspects of safety of graphene-based non-aqueous electrochemical supercapacitors: a case study with MgO-decorated few-layer graphene as an electrode material, New J. Chem. 43 (2019) 9793–9801, https://doi.org/10.1039/C9NJ00991D.
[53] S. Petnikota, G. Simões Dos Reis, F.A. Kayakool, V.S.S.S. Vadali, J. Välikangas, U. Lassi, M. Thyrel, Microwave Exfoliated Few-Layered Graphene Cathode for Aluminum Batteries, ACS Appl. Energy Mater. 7 (2024) 6862–6872, https://doi.org/10.1021/acsaem.4c00444.
[54] F. Sun, D. Wu, J. Gao, T. Pei, Y. Chen, K. Wang, H. Yang, G. Zhao, Graphitic porous carbon with multiple structural merits for high-performance organic supercapacitor, J. Power Sources 477 (2020) 228759, https://doi.org/10.1016/j.jpowsour.2020.228759.
[55] T. Huang, F. Wen, Y. Zheng, F. Fu, H. Li, L. Chen, D. Yang, Y. Wu, W. Zhang, Building mesoporous channels in lignin-derived microporous carbons to remold the electrochemical behaviors of supercapacitors, J. Power Sources 621 (2024) 235328, https://doi.org/10.1016/j.jpowsour.2024.235328.
[56] Q.D. Nguyen, J. Patra, C.-T. Hsieh, J. Li, Q.-F. Dong, J.-K. Chang, Supercapacitive Properties of Micropore- and Mesopore-Rich Activated Carbon in Ionic-Liquid Electrolytes with Various Constituent Ions, ChemSusChem. 12 (2019) 449–456, https://doi.org/10.1002/cssc.201802489.
[57] V.N. Kitenge, D.J. Tarimo, G. Rutavi, V.M. Maphiri, S. Sarr, M. Diop, M. Chaker, N. Manyala, Influence of nitrogen and sulfur co-doped activated carbon used as electrode material in EmiFSI ionic liquid toward high-energy supercapacitors, J. Energy Storage 81 (2024) 110453, https://doi.org/10.1016/j.est.2024.110453.
[58] W. Liu, X. Yan, J. Lang, Q. Xue, Effects of concentration and temperature of EMIMBF4/acetonitrile electrolyte on the supercapacitive behavior of graphene nanosheets, J. Mater. Chem. 22 (2012) 8853–8861, https://doi.org/10.1039/C2JM15537K.
[59] P. Chang, J. Zheng, Y. Cen, F. Yang, X. Li, Q. Xie, J. Dong, 3D hierarchical porous carbon from fulvic acid biomass for high energy density supercapacitor with high withstanding voltage, J. Power Sources 533 (2022) 231413, https://doi.org/10.1016/j.jpowsour.2022.231413.
[60] J.H. Kim, Y. Ko, Y.A. Kim, K.S. Kim, C.-M. Yang, Sulfur-doped carbon nanotubes as a conducting agent in supercapacitor electrodes, J. Alloys Compd. 855 (2021) 157282, https://doi.org/10.1016/j.jallcom.2020.157282.
[61] G. Li, A. Iakunkov, N. Boulanger, O.A. Lazar, M. Enachescu, A. Grimm, A. V. Talyzin, Activated carbons with extremely high surface area produced from cones, bark and wood using the same procedure, RSC. Adv. 13 (2023) 14543–14553, https://doi.org/10.1039/D3RA00820G.
[62] N. Boulanger, A.V. Talyzin, S. Xiong, M. Hultberg, A. Grimm, High surface area activated carbon prepared from wood-based spent mushroom substrate for supercapacitors and water treatment, Colloids Surfaces A Physicochem. Eng. Asp. 680 (2024) 132684, https://doi.org/10.1016/j.colsurfa.2023.132684.
[63] A. Nordenström, N. Boulanger, A. Iakunkov, G. Li, R. Mysyk, G. Bracciale, P. Bondavalli, A.V. Talyzin, High-surface-area activated carbon from pine cones for semi-industrial spray deposition of supercapacitor electrodes, Nanoscale Adv. 4 (2022) 4689–4700, https://doi.org/10.1039/D2NA00362G.